Maejo Int. J. Sci. Technol. **2016**, *10*(02), 220-232

Maejo International Journal of Science and Technology

ISSN 1905-7873
Available online at www.mijst.mju.ac.th

Full Paper

Exploiting distance metrics-based similarity for spatial feature analysis: Application to brain magnetic resonance imaging

Luminița Moraru [1, *], Simona Moldovanu [1, 2], Mirela (Vișan) Punga [1, 3], Stephen Johnson [4, 5] and Anjan Biswas [4, 6]

[1] Department of Chemistry, Physics and Environment, Faculty of Sciences and Environment, Dunarea de Jos University of Galati, 47 Domneasca St., 800008, Romania
[2] Dumitru Motoc High School, 15 Milcov St., 800509, Galati, Romania
[3] Aurel Vlaicu High School, 1 Decembrie 1918 St., 800511, Galati, Romania
[4] Department of Mathematical Sciences, Delaware State University, Dover, DE 19901-2277, USA
[5] Lake Forest High School, 5407 Killens Pond Road, Felton, DE 19943, USA
[6] Department of Mathematics, Faculty of Science, King Abdulaziz University, Jeddah-21589, Saudi Arabia
* Corresponding author, e-mail: luminita.moraru@ugal.ro

Received: 17 February 2015 / Accepted: 2 August 2016/ Published: 17 August 2016

Abstract: The well-known degenerating neurological diseases that cause dementia include Alzheimer's disease (AD), Huntington's disease (HD) and Pick's disease (PD). The spatial features of whole-brain neuroimages depicted by AD, HD and PD diseases have been little explored and thus allow new directions in research. In this study we explore the possibility of distinguishing between patients with neurological disorders and the healthy or normal cognitive (NC) elderly, paying special attention to statistical similarity measurements through histogram analysis. The whole-brain spatial histogram and 2D-texture-descriptor local binary pattern based on rotation invariance are utilised. The histogram comparison by means of the probability of different grey-level appearance needs less computational requirements and has satisfactory recognition accuracy. Various pseudo-metrics for comparing histogram distributions, as well as the data from 21 NC, 24 AD, 18 HD and 16 PD brain magnetic resonance images, were used. The statistical analysis, which is associated with correlation and concordance correlation coefficients, compares pairs of diseases in order to assess the effectiveness of texture features in differentiating between patients with dementia and the healthy elderly.

Keywords: degenerative neurological diseases, texture analysis, distance metrics, spatial feature analysis, brain magnetic resonance images

Maejo Int. J. Sci. Technol. **2016**, *10*(02), 220-232

INTRODUCTION

From the imaging techniques' point of view, aging is also associated with alterations in tissue intensity and contrast. Normal aging leads to atrophy of the grey matter and white matter as well as an increase in the cerebro-spinal fluid [1, 2]. Prince et al. [3] estimated that 35.6 million people lived with dementia worldwide in 2010. In the upcoming 20 years this number will almost double. It is estimated that in 2030 about 65.7 million people will be affected by dementia. Also, they have shown that in 2010, 58% of all people with dementia lived in countries with low or middle incomes, and they anticipate an increase of up to 63% in 2030 and 71% in 2050. Additionally, the elderly population is expected to double by 2030, and it is well known that dementia prevalence increases with age. Greater attention and particular concern are given to dementia because the decline in memory and other cognitive functions leads to a substantial impact on individuals, families and healthcare systems.

In this study we propose a method to distinguish those with dementia disorders (as Alzheimer's, Huntington's and Pick's diseases) from the healthy or normal cognitive (NC) elderly based on statistical similarity measurements through histogram analysis. This method belongs to the diagnosis-facilitating techniques. Alzheimer's disease (AD) is a neurological disorder with a severe loss of memory and cognitive abilities and characterised by a gradual onset and worsening of symptoms [4]. Generally, people aged 65 years or older are affected. The average lifespan after diagnosis is typically about 8 years [5, 6]. Cuingnet et al. [7] reported a comparative study of different methods for sophisticated feature selection in the classification of patients with AD based on anatomical magnetic resonance (MR) images. The goal was to assist in the early diagnosis of AD. The authors concluded that those methods did not perform substantially better than simpler ones. Also, they found that the oldest controls and the youngest patients were more often misclassified. AD today remains incurable but it is vital for patients to receive an effective treatment to slow down the progression of symptoms, improve life quality and extend life expectancy. Huntington's disease (HD) is an inherited, degenerative brain disease that affects the mind and body. It usually begins during mid-life, and both the intellectual decline and irregular and involuntary movements of the limbs or facial muscles are the specific features. Image analysis does not provide much information on this disease. Majid et al. [8] analysed T1-weighted structural scans to evaluate the neural degeneration in the pre-manifest stage of HD. Their focus was on the contribution of biomarkers in atrophy detection that is consistent with the known pre-manifest stage of HD. Pick's disease (PD) is a rare brain disorder, characterised morphologically by severe atrophy of the tissues in the frontal and temporal lobes of the brain and by the presence in the cerebral cortex of degenerative neuronal lesions or abnormal bodies (Pick's bodies). PD usually begins between the ages of 40-60. The symptoms are similar to AD.

Texture analysis (TA) technique provides a means of obtaining tissue information such as the features of being smooth or rough, regular or irregular and coarse or fine, and the random appearance patterns. Texture features can be used to characterise the properties of tissues or to detect structural abnormalities in different tissues [9, 10]. The discriminative power of TA in the diagnosis of degenerating neurological diseases that cause dementia has not been largely studied. At the early stage of research, co-occurrence matrix-based TA has been found to be sensitive in differentiating AD patients from NC persons [11]. Later, Li et al. [12] found that the features extracted from MR images using co-occurrence matrices could be correlated with the scores of the mini mental-state exam, which is a test of cognitive impairments typically used in AD medical

diagnosis. Bicacro et al.[13] successfully used histograms of the gradient magnitude and orientation and Haar-like features to extract the texture of deoxy-D-glucose positron emission tomographic images in order to distinguish between AD patients, patients with mild cognitive impairment and NC persons. Gray et al. [14] explored previous knowledge about the disease in order to segment the regions that are typically affected by AD. Only the average intensities of such regions of interest were used as features. Lillemark et al. [15] used both the surface connectivity marker and centre of mass-based marker as tools for the classification of NC, mildly-impaired cognitive, and AD subjects. The surface connectivity marker could detect mild cognitive impairment by means of an area under the curve of 0.599 for the 1-year period. Illán et al. [16] proposed a fully automatic computer-aided diagnosis system in order to improve the accuracy of early diagnosis of AD. The final classification was based on an automatic feature selection. Also, a combination of component-based support vector machine classification and a pasting vote technique that combines an unweighed sum of votes with the relevant information contained in the analysed areas was used.

Each MR image has an intensity that reflects both the physiological state of the tissues and impact of the diseases [17]. Any variation of the spatial intensity distribution results in an abnormal scan. Apparently, the histogram technique that measures the frequency of occurrence of the different grey-scale patterns throughout the image is an attractive method to assess and characterise the texture of an image. In practice, the number of entries in the histogram is so large that even for small neighbourhoods it is impossible to take into account all the possible patterns. The simplest way to overcome this drawback is by decreasing the number of grey levels. The Local Binary Pattern (LBP) method represents a proper solution [18, 19].

In this paper we focus on the LBP method. In the last decade the LBP application in the medical field has been limited to adenoma detection in endoscopic images and nodular thyroid segmentation in ultrasound images [20, 21]. Oppedal et al. [22] used the 2D-LBP method to extract the textural information of white matter lesions in MR images in order to diagnose different types of dementia including, but not restricted to, AD. The LBP is a grey-scale invariant local texture descriptor with minimal computational complexity. Recently, LBP was used to include prior information about the localisation of changes in the human brain and to differentiate AD versus NC groups by using a support vector machine [23, 24]. Chang et al. [25] used isotropic LBPs on three orthogonal planes to distinguish between attention deficit and hyperactivity disorders based on morphological information without using functional data. They used various parcellations and different image resolutions but their conclusion was that parcellation information did not improve the results. Also, the LBP method avoids a course of dimensionality [26, 27].

As a step forward, our goals are to detect global differences in spatial patterns in patients suffering from degenerating neurological diseases that cause dementia and to analyse the texture dissimilarity between healthy brains and those affected by dementia. More precisely, we use the well-known descriptor, LBP, for texture extraction and histogram comparison. The relative differences between histograms can be quantified across different pathological subjects and act as an indicator for differentiating dementia from NC subjects, and can also lead to an early detection of the degenerating neurological diseases.

The main purpose of this work is to develop a method with less computational complexity but good enough to work equally efficiently for various data sets. The specific objectives of this study are: 1) to determine the existing structural changes relative to NC subjects; 2) to use various pseudo-metrics for comparing histogram distributions; and 3) to use the well-known statistical

procedures (involving the use of correlation and concordance correlation coefficients) for a paired comparison of results across the data set.

MATERIALS AND METHODS

Data Sets and Data Processing

The brain atlas images used in this study were retrieved from the Harvard Medical School database [28]. A series of T2-weighted MR slices in 2D format belonging to four different MR image data sets were used in the experiments. In total, 21 MR images of the healthy (or NC) elderly, 24 AD patients, 18 HD patients and 16 PD patients were used. Slices from the axial plane and 256 × 256 in-plane resolution were carefully selected in terms of position, orientation and scale of the reference NC images and the images corresponding to AD, HD and PD. Within the sequence 2D+T, similar slices (i.e. those placed at the same level) were selected. A flow chart of the data analysis procedure is shown in Scheme 1. We implemented the proposed technique by means of MATLAB.

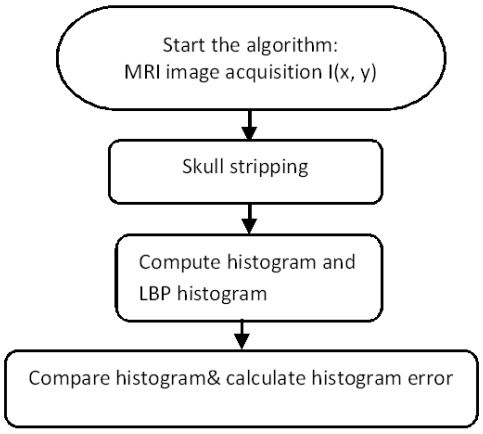

Scheme 1. Flow chart of data analysis procedure

Preprocessing: Skull Stripping

We develop our own method of eliminating outward bone rings (skull-stripping), while the white matter, grey matter and cerebro-spinal fluid should remain intact in the brain MR image obtained. The skull-stripped brains are the input for the LBP algorithm and histogram comparison. In our algorithm the brain and non-brain regions are automatically identified by means of a mask produced by segmentation and morphological operations. This mask includes brain tissues and eliminates the skull, skin, muscles, fat, eyes, dura mater and bone. The background or non-mask tissues is associated with zero intensity. The foreground or mask (including cerebral matter) gets all the non-zero intensity of pixels. Then an image-subtraction algorithm for the original image against the masked image is used. Figure 1 shows some samples of the skull-stripped MR images of the brain used in the experiments.

The Dice similarity metric was used to assess the segmentation results [29]. The average Dice scores of 0.9645±0.0272 for NC, 0.9605±0.0072 for AD, 0.9471±0.0312 for HD and 0.9276±0.0092 for PD were computed.

Maejo Int. J. Sci. Technol. **2016**, *10*(02), 220-232

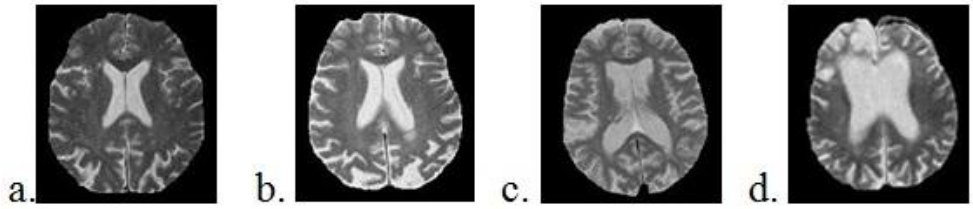

Figure 1. Samples of skull stripped brain MR images: (a) NC; (b) AD; (c) HD; (d) PD

Two-dimensional LBP

The LBP is a texture operator used to convert the pixels into an image by thresholding the neighbourhood of each pixel and converting the result into a binary number. Since the brain MR images are strongly affected by non-uniform illumination, the robust invariance against the monotonic grey level of the LBP makes it a good texture operator. The LBP acts on every local region uniformly. It encodes the texture of the local neighbourhood of a given pixel $X_c = (x_c, y_c)$ in a 3 × 3 neighbourhood, using the central value as a threshold. The encryption is done by multiplying the threshold values by weights given by the corresponding pixels and then summing up the result. Each peripheral pixel of the 3 × 3 neighbourhood is assigned a value 0 or 1 if its grey-level intensity is below or above the intensity of the central pixel respectively. As the neighbourhood consists of 8 pixels, if the grey value of the central pixel and the neighbouring pixels are considered, a total of $2^8 = 256$ different labels can be obtained. The kernel function is

$$f_{LBP}(X_c) = \sum_{j=0}^{7} 2^j (I_j - I_c) \quad (1)$$

where I_c is the grey level of the central pixel and I_j the grey levels of the peripheral pixels $j \in \{0, 1,..,7\}$.

After computing the LBPs associated with all pixels (by sliding the mask over the image), the texture of the image is extracted by means of the histogram. However, the number of distinct patterns grows exponentially with the number of sampling points ($\sim 2^j$) and the practical estimation of the genuine occurrence probabilities is very difficult. In this case the histogram stability has become a serious issue because if we assume that there are 24 neighbours for the central pixel, then more than 16 million patterns exist. To overcome this drawback, a rotation-invariant LBP (RI-LBP) operator has been introduced [19, 30]. It reduces the feature vector length of the LBP needed in the texture analysis and is less sensitive to variances in rotation, scale and illumination. The RI-LBP descriptor is obtained by converting the squared 3 × 3 mask into a circular neighbourhood indicated as (8; 1). The circle is centred at the central pixel of the mask. The first number is the number of pixels at the periphery and the second is the radius of the circle (in pixels). The peripheral pixels' location is dependent on the central pixel position, and the localisation at non-integer pixel coordinates can exist. Here, a bi-linear interpolation is used. In the second step the feature vector is processed to obtain another vector which is invariant with the discrete rotations of the input image.

Texture Analysis

It is well known that different regions of the brain may consist of different textures. We adopted a local texture analysis by using local signal processing that maximises the separation and discrimination among different texture representations. The LBP feature extraction algorithm represents an image as a sum of LBP histograms. Each LBP histogram is extracted from a local

Maejo Int. J. Sci. Technol. **2016**, *10*(02), 220-232

region of the image. Large structural differences in the cerebral cortex are searched and different histograms are computed for different diseases. These histograms are a good descriptor for the comparison of changes among images. However, the dimensionality of the input data is large and the number of bins in a histogram grows exponentially with the number of the input data. To overcome this drawback, a sparse representation of the histograms is used; only those bins whose content is not empty are stored.

Experimental Design

Our experiments were carried out using the same parameters for every problem. Iakovidis et al. [20] showed that the pair (p; r) = (8; 1) is a good compromise between classification accuracy and boundary errors. Here, p specifies the number of neighbours and the number of enabled filter elements; r = 1 is the radius of the neighbourhood sizes of 3 × 3. The implementation steps are as follows: 1) a radial filter to compare the central pixel with the pixel of the immediate proximity and a logical operation that generates the RI-LBP are used. This increases the running time but it results in a relatively sparse histogram (many combinations disappear). Here, all neighbours receive similar treatment; 2) a function is used to modify the contrast of the input images by replacing the pixel values in a manner that results in either a tight histogram (with no empty bins) or a uniformly distributed histogram; 3) a logical function provides the output array. It does not contain repeated elements and the element order is not altered.

Histogram Matching

One histogram for each brain MR image was built to represent the texture region. To prove useful in classification problems, the information provided by the histograms must be combined in a certain manner. In order to estimate the similarity/dissimilarity between two images, the histogram of NC individuals was compared with those of the AD, HD and PD patients using various standard distance metrics [31]. Four measures of similarity between demented and normal brain slices were used. Two particular cases of the Minkowski distance $d_{MKW}(i,j) = \sqrt[\lambda]{\sum_{k=0}^{n-1}\left|y_{i,k} - y_{j,k}\right|^{\lambda}}$ were analysed. Here, y denotes the variables in the dataset, k is the index of the variable, n is the total number of variables and λ is the order of the Minkowski metric; λ = 1 corresponds to the Manhattan distance and λ = 2 to the Euclidean distance. In equations 2-5, D1 denotes the Euclidian distance, D2 is the Euclidean squared distance and D3 is the Manhattan distance; they are metric similarity functions. D4 denotes the vector cosine angle distance and it is a non-metric similarity function. D1, D2 and D3 indicate the magnitude of difference between two vectors while D4 gives a measure of how similar the two vectors are, but with no regard to magnitude.

$$D1(h_{dis}, h_{NC}) = \sqrt{\sum_i (h_{dis}(i) - h_{NC}(i))^2} \quad (2)$$

$$D2(h_{dis}, h_{NC}) = \sum_i (h_{dis}(i) - h_{NC}(i))^2 \quad (3)$$

$$D3(h_{dis}, h_{NC}) = \sum_i |h_{dis}(i) - h_{NC}(i)| \quad (4)$$

$$D4(h_{dis}, h_{NC}) = \sum_i h_{dis}(i) \cdot h_{NC}(i) \Big/ \sqrt{\sum_i h_{dis}^2(i)} \cdot \sqrt{\sum_i h_{dis}^2(i)} \quad (5)$$

Maejo Int. J. Sci. Technol. **2016**, *10*(02), 220-232

Here, h_{dis} and h_{NC} are the histograms of demented and normal brain images respectively. All these metrics are non-negative and measure the similarity score. Scores closer to 0 indicate a more perfect similarity between slices. All T2-weighted MR images were spatially normalised.

Statistical Analysis

After collecting the experimental data, the first compulsory step is to identify the values affected by aberrant errors. These data are eliminated. The identification of the data affected by aberrant errors is accomplished by applying the Chauvenet test [31].

For statistical studies and inter-patient correlation, the similarity degree of histograms is based on a pair analysis. The linear correlation coefficient r and the coefficient of determination r^2 were computed for each pair of data sets. The quantity r measures the strength and direction of a linear relationship between two variables, and the quantity r^2 gives the proportion of the variance (fluctuation) of one variable that is predictable from the other variable. Also, it indicates how certain one can be in making predictions from a certain investigation.

In order to understand the significance of individual independent variables and measure how well a new set of observations reproduces an original set, the concordance correlation coefficient (CCC) [32] was used:

$$CCC = 2r\sigma_1\sigma_2 / \left(\sigma_1^2 + \sigma_2^2 + (\mu_1 - \mu_2)^2\right) \quad (6)$$

where (μ_1, μ_2) and (σ_1^2, σ_2^2) are the means and variances of the data sets S1 and S2 respectively. In order to assess the reproducibility and the similarity/dissimilarity of the results, CCC was applied to both the spatial histogram and RI-LBP histogram analysis.

RESULTS AND DISCUSSION

We have encountered serious difficulties during our similarity/dissimilarity studies based on grey level intensity due to the scarcity of HD and PD image databases as well as differences in image resolution, slice thickness and image quality. The methodology applied in this study aims to quickly identify dementia in MR images. As the first step, a histogram comparison is performed, which shows the relative frequencies of occurrence of each pattern of the diseases analysed compared with the NC brain images. Figure 2 shows examples of some disease pairs. Afterwards, the histograms of all 2^p LBP labels and the RI-LBP components are computed and used as texture descriptors and also for comparison purposes. Some pairs of images are shown in Figures 3 and 4. The average similarity score values, the standard deviations and the statistics associated with the histogram comparisons are shown in Tables 1-4.

In the case of HD, some aberrant values were found and eliminated. Only the minimum values in the array of the histograms were affected. About 6% of the bins were classified as outliers according to the Chauvenet criterion.

According to the data in Tables 1-3, we can conclude that all dementia diseases clearly are statistically different as the D1, D3 and D4 similarity scores are not equal to 0. D2 does not perform well and it was removed from our analysis. High D3 values exhibit the highest dissimilarity. The linear regression analysis of different pairs of analysed samples results in the correlation coefficients ranging from 0.72 to 0.99. The coefficient of determination shows how close the data are to the fitted regression line. It ranges between 0.53 and 0.97. The drawback of the correlation coefficients is that they only take into account the linear dependency between a given feature and

Maejo Int. J. Sci. Technol. **2016**, *10*(02), 220-232

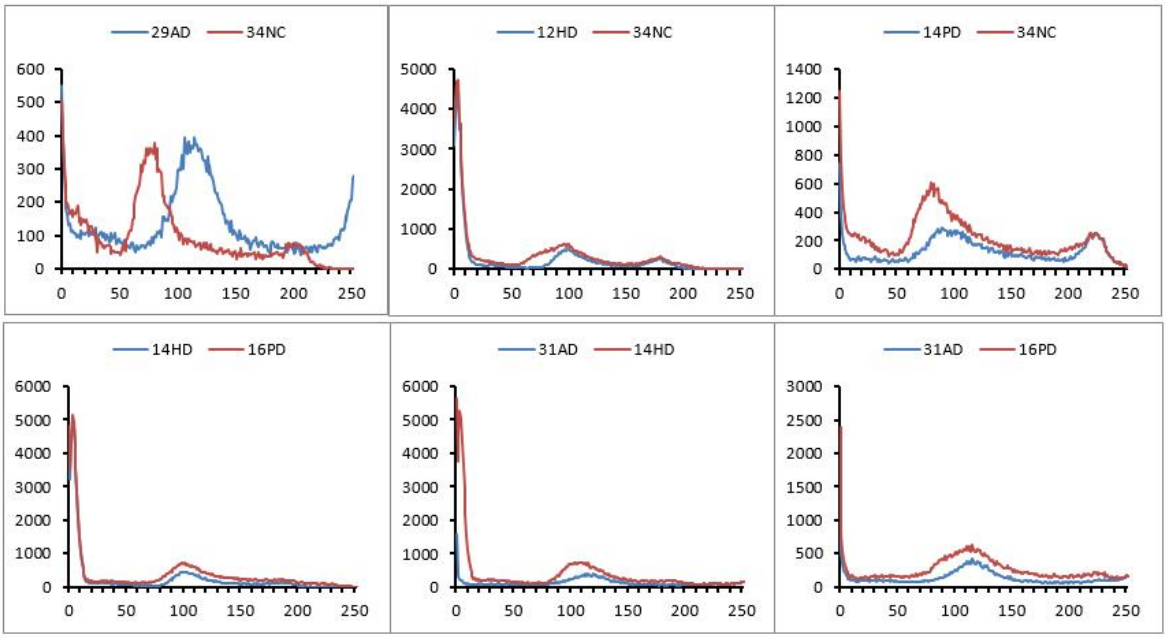

Figure 2. Examples of spatial histogram comparison. The paired slices are carefully selected in terms of position, orientation and scale between NC and AD, HD and PD cases. (x-Axis shows range of pixel values; y-axis counts pixels' intensities.)

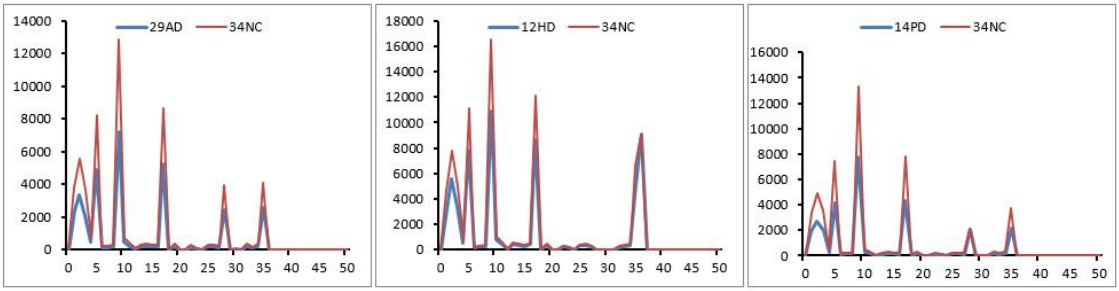

Figure 3. Examples of RI-LBP sparse histogram comparison (x-axis shows range of pixel values; y-axis counts pixels' intensities.)

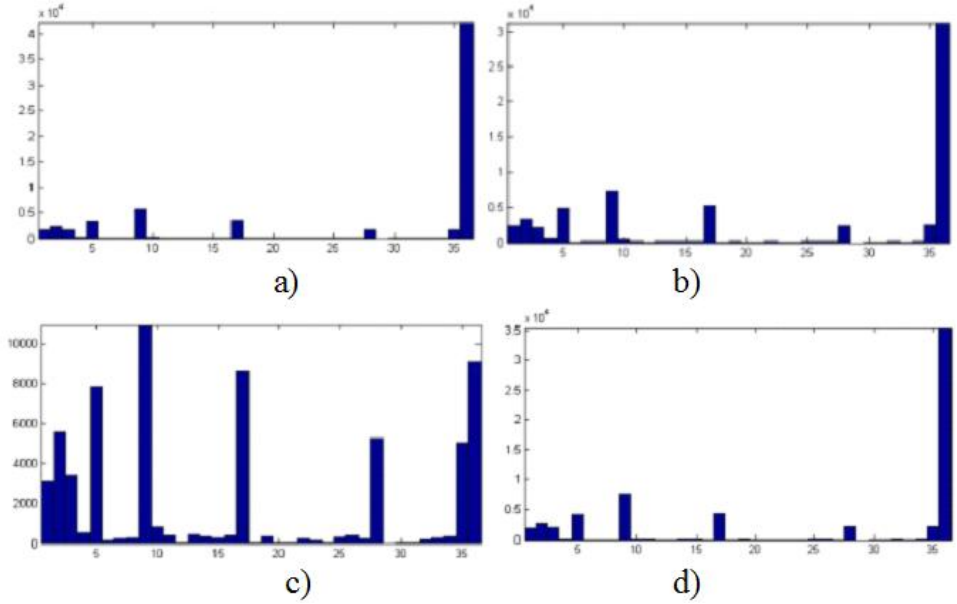

Figure 4. Examples of input histogram and feature sub-selection using LBP algorithm. RI-LBP tight histogram comparison for bins 1-35: a) NC; b) AD; c) HD; d) PD (x-axis shows range of pixel values; y-axis counts pixels' intensities.)

Maejo Int. J. Sci. Technol. **2016**, *10*(02), 220-232

Table 1. Statistical significance of histogram correlation regarding similarity scores between AD and NC cases

Similarity score	Mean		Standard deviation		Correlation coefficient r		Coefficient of determination r^2	
	Spatial	RI-LBP sparse	Spatial	RI-LBP sparse	Spatial	RI-LBP sparse	Spatial	RI-LBP sparse
D1	0.9130	0.1717	0.0115	0.0040	-0.8244	-0.8370	0.6797	0.7007
D2	0.0373	0.0288	0.0004	0.0023	-0.7551	-0.9741	0.5702	0.9490
D3	0.5810	0.3239	0.0438	0.0132	-0.8419	-0.7944	0.7089	0.6311
D4	0.3328	0.3136	0.0218	0.0359	-0.9987	-0.9889	0.9775	0.9780

Table 2. Statistical significance of histogram correlation regarding similarity scores between HD and NC cases

Similarity score	Mean		Standard deviation		Correlation coefficient r		Coefficient of determination r^2	
	Spatial	RI-LBP sparse	Spatial	RI-LBP sparse	Spatial	RI-LBP sparse	Spatial	RI-LBP sparse
D1	0.5977	0.5532	0.0201	0.0211	+0.9688	+0.9790	0.9386	0.9586
D2	0.0111	0.3065	0.0009	0.0235	-0.9017	+0.9778	0.8132	0.9561
D3	1.3439	1.0632	0.0258	0.0397	+0.7842	+0.7293	0.6150	0.5320
D4	0.4466	0.4102	0.0113	0.0201	-0.9778	-0.9796	0.9562	0.9598

Table 3. Statistical significance of histogram correlation regarding similarity scores between PD and NC cases

Similarity score	Mean		Standard deviation		Correlation coefficient r		Coefficient of determination r^2	
	Spatial	RI-LBP sparse	Spatial	RI-LBP sparse	Spatial	RI-LBP sparse	Spatial	RI-LBP sparse
D1	0.1980	0.1674	0.0229	0.0216	-0.9753	-0.9678	0.9513	0.9368
D2	0.0131	0.0598	0.0007	0.0099	-0.9331	-0.9820	0.8708	0.9644
D3	0.3989	0.2808	0.0512	0.0387	-0.8743	-0.9792	0.7645	0.9589
D4	0.2500	0.2663	0.0085	0.0187	-0.9786	-0.9837	0.9578	0.9678

Table 4. Average values of CCC for the cases under analysis

	Histogram	RI-LBP histogram
NC vs. AD	0.9962	0.9895
NC vs. HD*	**0.3051**	**0.5662**
NC vs. PD	0.9992	0.9952
AD vs. PD	0.9964	0.9968
AD vs. HD*	**0.3767**	**0.6944**
HD vs. PD*	**0.3536**	**0.6419**

* The cases where the null hypothesis is rejected are denoted by the numbers in bold

Maejo Int. J. Sci. Technol. **2016**, *10*(02), 220-232

the class label. An improved measure of information dependency (or degree of concordance between the two measures) arises from the concordance correlation coefficient (Table 4).

Our null hypothesis of the comparison test is that the image variables are independent of the health condition (NC case). The data for NC vs. AD, NC vs. PD and AD vs. PD indicate that the differentiation is significantly realistic at 5% confidence level. For the cases NC vs. HD, AD vs. HD and HD vs. PD, at any reasonable confidence level, the null hypothesis is rejected. There is sufficient evidence to indicate the impossibility of differentiating between HD and the rest of the samples under analysis, even if the results have been improved in the case of RI-LBP.

The CCC quantifies the agreement between two measures of the same variable. This data analysis strategy allows us to simplify the texture analysis approach when there is a concordance correlation between the grey level intensities of the bins, or to reveal the disagreement between them. Although all the dementia diseases analysed are characterised by changes in tissue volume and structure, our results based on histogram comparison by means of the probability of different grey-level appearance for dissimilarity studies are found to be accurate in discriminating between AD, PD and NC subjects. Two textural surfaces are significantly dissimilar if the test fails to reject the null hypothesis of resemblance, or resemble each other if the null hypothesis is rejected. The pairs NC vs. AD, NC vs. PD and AD vs. PD demonstrate considerable equivalent correlations and acceptable values for D1, D3 and D4 similarity scores. Despite the fact that D3 has higher values, which points to the highest dissimilarity for HD, the pairs NC vs. HD, AD vs. HD and HD vs. PD exhibit lower concordance.

Notably, after applying the RI-LBP operator, there is no significant difference between results in the cases of NC vs. AD, NC vs. PD and AD vs. PD, although there is an improvement for HD vs. NC, AD and PD. The CCC values increase when the rotation invariance and uniformity are introduced to the LBP. This observation is coherent with the fact that the rotation invariance and the uniform LBP patterns correspond to the primitive micro-features of the image (such as edges, corners and spots) [19]. Models using histograms computed from the whole-brain region show higher accuracy for AD and PD. Thus, the measures of association seem to carry many of the important differences between AD and PD, which is consistent with prior findings [8, 33].

An important issue needs to be specified. The brain MR images of all patients already have the same orientation (slides in axial view were analysed), so the rotation invariance is not used to achieve the maximum possible discrimination. It only allows the reduction of the number of possible patterns. Meanwhile, the histogram analysis clearly indicates its discriminative potential in this study. The histogram descriptor has different signatures for different neurological degenerative diseases, which shows its discriminative ability in the classification task.

Following the results reported by Montagne et al. [23], we use the distribution of whole-brain features. These authors reported lower accuracy for the test parcellation or region-of-interest strategies. Our results indicate that histograms computed from the whole-brain region show higher accuracy than models based on the region-of-interest extraction.

Our results are based on the regional morphological brain changes. It is well known that the parts of the brain affected by HD are a group of nerve cells at the base of the brain known as basal ganglia (whose major components are the caudate nuclei, putamen and pallidum subcortical nuclei), the frontal and temporal lobes, and the ventricles. In the case of AD, shrinkage is especially severe in the hippocampus, and in addition the ventricles (fluid-filled spaces within the brain) grow larger. PD or fronto-temporal dementia affects the frontal and/or temporal lobes of the brain. According to Gemmell et al. [34] and Giorgio et al. [35], hippocampal atrophy does not strictly occur during the

normal aging processes, but is also manifest in AD. These specific regions of the brain that are usually affected by the dementia diseases under study are the answer to our attempt to differentiate the type of disease.

Our approach based on structural images and spatial context information shows potential use in the clinical environment, although we clearly state that this method alone cannot be used to diagnose the types of dementia. A diagnosis can be made if MR scans can ascertain the histogram pattern of morphological brain changes. Nevertheless, the method can assist radiologists and neurologists by identifying spatial grey level intensity models producing similar and dissimilar results, and thereby may help to validate clinical findings. This work can of course be improved in the future.

CONCLUSIONS

In this paper we have focused on a quite simple and quick method that can inform the end user about the differences in the textures of brain MR images showing different dementia diseases. Joint RI-LBP and intensity histograms are used to characterise whole brain images. The RI-LBP performs slightly better than the spatial histogram. A simple statistical analysis appears to be sufficient for this comparative analysis. We do not claim that our study is entirely consistent, but we further expect to increase its relevance by enlarging the image database. At this moment, there are large and very well documented databases for AD, but HD and PD are less represented in MR image databases. The role of neuroscientists of course remains crucial. They provide their scientific judgment based on a wide range of symptoms. However, signal processing and statistical methods have gained an increasing role in MR imaging in neuroscience and spatial texture features remain a powerful tool in revealing complex patterns of brain surfaces.

ACKNOWLEDGEMENTS

The second author (S.M.) would like to thank Project PERFORM, ID POSDRU/159/1.5/S/138963 of "Dunărea de Jos", University of Galati, Romania for the support. The third author (M.V.P) would like to thank Project ExcelDOC, ID POSDRU/159/1.5/S/132397 of "Dunărea de Jos", University of Galati, Romania for the support.

REFERENCES

1. C. D. Good, I. S. Johnsrude, J. Ashburner, R. N. Henson, K. J. Friston and R. S. Frackowiak, "A voxel-based morphometric study of ageing in 465 normal adult human brains", *Neuroimage*, **2001**, *14*, 21-36.
2. D. H. Salat, R. L. Buckner, A. Z. Snyder, D. N. Greve, R. S. Desikan, E. Busa, J. C. Morris, A. M. Dale and B. Fischl, "Thinning of the cerebral cortex in aging", *Cereb. Cortex*, **2004**, *14*, 721-730.
3. A. Fernández, M. X. Álvarez and F. Bianconi, "Texture description through histograms of equivalent patterns", *J. Math. Imaging Vision*, **2013**, *45*, 76-102.
4. P. M. Doraiswamy, L. Kaiser, F. Bieber and R. L. Garman, "The Alzheimer's disease assessment scale: Evaluation of psychometric properties and patterns of cognitive decline in multicenter clinical trials of mild to moderate Alzheimer's disease", *Alzheimer Dis. Assoc. Disord.*, **2001**, *15*, 174-183.

5. R. Brookmeyer, S. Gray and C. Kawas, "Projections of Alzheimer's disease in the United States and the public health impact of delaying disease onset", *Am. J. Pub. Health*, **1998**, *88*, 1337-1342.
6. R. Brookmeyer, M. M. Corrada, F. C. Curriero and C. Kawas, "Survival following a diagnosis of Alzheimer disease", *Arch. Neurol.*, **2002**, *59*, 1764-1767.
7. R. Cuingnet, E. Gerardin, J. Tessieras, G. Auzias, S. Lehéricy, M. O. Habert, M. Chupin, H. Benali and O. Colliot, "Automatic classification of patients with Alzheimer's disease from structural MRI: a comparison of ten methods using the ADNI database", *Neuroimage*, **2011**, *56*, 766-781.
8. D. S. Majid, D. Stoffers, S. Sheldon, S. Hamza, W. K. Thompson, J. Goldstein, J. Corey-Bloom and A. R. Aron, "Automated structural imaging analysis detects premanifest Huntington's disease neurodegeneration within 1 year", *Mov. Disord.*, **2011,** *26*, 1481-1488.
9. S. Zhou, J. Shi, J. Zhu, Y. Cai and R. Wang, "Shearlet-based texture feature extraction for classification of breast tumor in ultrasound image", *Biomed. Signal Process. Control*, **2013**, *8*, 688-696.
10. P. Morgado, M. Silveira and J. S. Marques, "Diagnosis of Alzheimer's disease using 3D local binary patterns", *Comput. Meth. Biomech. Biomed. Eng. Imaging Visual.*, **2013**, *1*, 2-12.
11. P. A. Freeborough and N. C. Fox, "MR image texture analysis applied to the diagnosis and tracking of Alzheimer's disease", *IEEE Trans. Med. Imaging*, **1998**, *17*, 475-478.
12. X. Li, H. Xia, Z. Zhou and L. Tong, "3D texture analysis of hippocampus based on MR images in patients with Alzheimer disease and Mild Cognitive Impairment", Proceedings of 3rd International Conference on Biomedical Engineering and Informatics, **2010**, Yantai, China, pp.1-4.
13. E. Bicacro, M. Silveira and J. S. Marques, "Alternative feature extraction methods in 3D brain image-based diagnosis of Alzheimer's disease". Proceedings of 19th IEEE International Conference on Image Processing, **2012**, Orlando, USA, pp.1237-1240.
14. K. R. Gray, R. Wolz, R. A. Heckemann, P. Aljabar, A. Hammers and D. Rueckert, "Multi-region analysis of longitudinal FDG-PET for the classification of Alzheimer's disease", *Neuroimage*, **2012**, *60*, 221-229.
15. L. Lillemark, L. Sørensen, A. Pai, E. B. Dam and M. Nielsen, "Brain region's relative proximity as marker for Alzheimer's disease based on structural MRI", *BMC Med. Imaging*, **2014**, *14*, 21 (doi: 10.1186/1471-2342-14-21).
16. I. A. Illán, J. M. Górriz, M. M. López, J. Ramírez, D. Salas-Gonzalez, F. Segovia, R. Chaves and C. G. Puntonet, "Computer aided diagnosis of Alzheimer's disease using component based SVM", *Appl. Soft Comput.*, **2011**, *11*, 2376-2382.
17. M. Yoshita, E. Fletcher, D. Harvey, M. Ortega, O. Martinez, D. M. Mungas, B. R. Reed and C. S. DeCarli, "Extent and distribution of white matter hyperintensities in normal aging, MCI, and AD", *Neurology*, **2006**, *67*, 2192-2198.
18. H. Zhou, R. Wang and C. Wang, "A novel extended local binary-pattern operator for texture analysis", *Inform. Sci.*, **2008**, *178*, 4314-4325.
19. T. Ojala, M. Pietikainen and T. Maenpaa, "Multiresolution gray-scale and rotation invariant texture classification with local binary patterns", *IEEE Trans. Pattern Anal. Mach. Intell.*, **2002**, *24*, 971-987.
20. D. K. Iakovidis, D. E. Maroulis and S. A. Karkanis, "An intelligent system for automatic detection of gastrointestinal adenomas in video endoscopy", *Comput. Biol. Med.*, **2006**, *36*, 1084-1103.

21. D. K. Iakovidis, E. G. Keramidas and D. Maroulis, "Fuzzy local binary patterns for ultrasound texture characterization", *Lect. Notes Comput. Sci.*, **2008**, *5112*, 750-759.
22. K. Oppedal, K. Engan, D. Aarsland, M. Beyer, O. B. Tysnes and T. Eftestol, "Using local binary pattern to classify dementia in MRI", Proceedings of 9th IEEE International Symposium on Biomedical Imaging, **2012**, Barcelona, Spain, pp.594-597.
23. C. Montagne, A. Kodewitz, V. Vigneron, V. Giraud and S. Lelandais, "3D local binary pattern for PET image classification by SVM application to early Alzheimer disease diagnosis", Proceedings of 6th International Conference on Bio-Inspired Systems and Signal Processing, **2013**, Barcelona, Spain, pp.145-150.
24. A. Kodewitz, S. Lelandais, C. Montagne and V. Vigneron, "Alzheimer's disease early detection from sparse data using brain importance maps", *Electron. Lett. Comput. Vision Image Anal.*, **2013**, *12*, 42-56.
25. C. W. Chang, C. C. Ho and J. H. Chen, "ADHD classification by a texture analysis of anatomical brain MRI data", *Front. Syst. Neurosci.*, **2012**, *6*, 66 (doi: 10.3389/fnsys.2012.00066).
26. X. Wang and K. K. Paliwal, "Feature extraction and dimensionality reduction algorithms and their applications in vowel recognition", *Pattern Recogn.*, **2003**, *36*, 2429-2439.
27. J. Asensio-Cubero, J. Q. Gan and R. Palaniappan, "Extracting optimal tempo-spatial features using local discriminant bases and common spatial patterns for brain computer interfacing", *Biomed. Signal Process. Control*, **2013**, *8*, 772-778.
28. K. A. Johnson and J. A. Becker, "The whole brain atlas", **1999**, http://www.med.harvard.edu/AANLIB/home.html (Accessed: November 2014).
29. D. W. Shattuck, G. Prasad, M. Mirza, K. L. Narr and A. W. Toga, "Online resource for validation of brain segmentation methods", *Neuroimage*, **2009**, *45*, 431-439.
30. T. Ojala, M. Pietikainen and T. Maenpaa, "Multiresolution gray-scale and rotation invariant texture classification with local binary patterns", *IEEE Trans. Pattern Anal. Mach. Intell.*, **2002**, *24*, 971-987.
31. J. R. Taylor, "An Introduction to Error Analysis", 2nd Edn., University Science Books, Sauselito, **1997**, pp.25-96.
32. L. I. Lin, "A concordance correlation coefficient to evaluate reproducibility", *Biometrics*, **1989**, *45*, 255-268.
33. R. A. Sadek, "Regional atrophy analysis of MRI for early detection of Alzheimer's disease", *Int. J. Signal Process. Image Process. Pattern Recogn.*, **2013**, *6*, 49-57.
34. E. Gemmell, H. Bosomworth, L. Allan, R. Hall, A. Khundakar, A. E. Oakley, V. Deramecourt, T. M. Polvikoski, J. T. O'Brien and R. N. Kalaria, "Hippocampal neuronal atrophy and cognitive function in delayed poststroke and aging-related dementias", *Stroke*, **2012**, *43*, 808-814.
35. A. Giorgio, L. Santelli, V. Tomassini, R. Bosnell, S. Smith, N. De Stefano and H. Johansen-Berg, "Age-related changes in grey and white matter structure throughout adulthood", *Neuroimage*, **2010**, *51*, 943-951.